DROPPING IN ELECTROSPINNING PROCESS
A General Strategy for Fabrication of Microspheres

by

Leigen LIU[a], Yan-Qing LIU[b], Yun-Yu LI[c], Yue SHEN[d], and Ji-Huan HE[b,e]*

[a] School of Textile Garment and Design, Changshu Institute of Technology, Changshu, China
[b] National Engineering Laboratory for Modern Silk, College of Textile and Clothing Engineering, Soochow University, Suzhou, China
[c] School of Textile Science and Engineering, Xi'an Polytechnic University, Xi`an, China
[d] School of Science, Xi'an University of Architecture and Technology, Xi'an, China
[e] School of Mathematics and Information Science, Henan Polytechnic University, Jiaozuo, China

Original scientific paper
https://doi.org/10.2298/TSCI191228025L

The dropping mechanism in the electrospinning process is elucidated. A moving jet becomes thinner at the initial stage due to the acceleration caused by the electrostatic force. When the jet diameter reaches a threshold, beyond which the jet breaks into drops and daughter jets, dropping occurs. The drops will finally form microspheres. Effects of applied voltage, flow rate, polymer's concentration, and receptor's distance on the dropping process are theoretically analyzed and experimentally verified. This paper gives a general strategy for fabrication of smooth fiber, microspheres, and their mixture.

Key words: *drug delivery, tissue engineering, separation, mathematical model, catalytic reaction, bubble electrospinning, super-fine coating, cosmetics*

Introduction

Microspheres are widely used in controlled release drug delivery systems, tissue engineering, wound dressing scaffolds, and their new applications appear every day, for example, super-fine coating, cosmetics, catalytic reaction, energy, separation and others [1]. Porous microsphere has even more applications in adsorption, stealth technology, and smart textile. The general approach to fabrication of microsphere is the well-known electrostatic spraying [2], its principle is almost same with that of electrospinning [3-13]. When we use an electrospinning set-up to fabricate fibers, we can often obtain microspheres at some special conditions. Many reports were given in open literature that when the concentration of a polymer solution decreased to a threshold, instead of fibers, microspheres were obtained, or sometimes microsphere-nanofiber membrane could be fabricated. In electro-spraying process, when the polymer concentration increases, continuous fibers can be obtained instead of microspheres. Though both electrospinning and electro-spraying can be used for fabrication of microspheres, its mechanism is not clear yet, conflicting explanations were appeared in literature. This paper aims at giving a theoretical analysis for the mechanism.

* Corresponding author, e-mail: hejihuan@suda.edu.cn

Dropping mechanism in the electrospinning

Dropping phenomena can be observed in everyday life, for examples, water drops falling from a tap, and drops from a honey filament. Honey is much more viscous than water, so it has a long journey before dropping. A similar phenomenon appears in a moving jet in the electrospinning.

Before dropping and solidification, the moving jet follows the mass conservation law. For 1-D steady flow ignoring solvent evaporation, the mass equation can be written:

$$\pi r^2 \rho u = Q \tag{1}$$

where u is the velocity of the jet, ρ – the density of the jet, r – the radius of the jet, and Q – the flow rate which is a constant in our study.

The jet ejecting from the Taylor cone is accelerated due to the electrostatic force, so the initial ejecting velocity is high, it can reach as high as 300 m/s in the bubble electrospinning [14], according to eq. (1), a higher velocity implies a smaller radius of the moving jet. Due to air drag and viscous resistance, the moving jet decelerates gradually.

As a qualitative analysis, we consider the jet as a Newtonian flow, the viscous resistance acting on the jet section:

$$T = \pi r^2 \mu \frac{\mathrm{d}u}{\mathrm{d}x} \tag{2}$$

where u is viscous coefficient.

When the moving jet decelerates until $\mathrm{d}u/\mathrm{d}x = 0$ or $\mathrm{d}u/\mathrm{d}x$ becomes extremely small, viscous resistance disappears completely or extremely small. Under such a condition, due to the inertia force, a drop will be ejected from the jet, and daughter jets might form during the dropping process, see fig. 1.

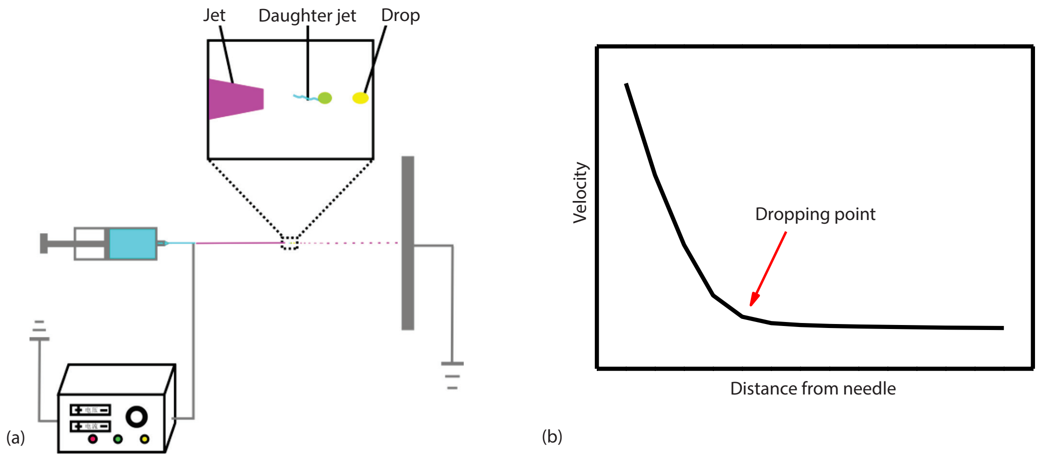

Figure 1. Dropping in a moving jet; (a) spinning-dropping processing, (b) when velocity gradient becomes zero, dropping occurs

According to the aforementioned analysis, dropping can occur for following three cases:
– viscous coefficient is small,
– the radius of the moving jet decreases fast, and
– velocity gradient is small $\mathrm{d}u/\mathrm{d}x \to 0$.

Figure 1(b) shows a spinning-dropping system, before the dropping point, spinning occurs; after the dropping point, dropping occurs. If the dropping point approaches to the needle point, spraying is predicted. Fibers can be obtained when the receptor is placed before the dropping point, and particles are produced when the receptor is placed after the dropping point.

Experiment design

A binary solvent system using dimethyl formamide (DMF) and acetone as solvents was prepared with a weight ratio: DMF/acetone = 7/3. Polyvinylidene fluoride (PVDF) (Minnesota Mining and Manufacturing Company, USA) and Polyether sulfones (PES) (American SOLVAY) were used without any purification. The PVDF powders were put into the DMF/acetone bi-solvent system in a sealed beaker to prepare for a PVDF solution by stirring the mixture magnetically (magnetic stirrer with the water temperature of 50 °C, DF-101S, Xinrui Instrument Co. Ltd.) for 2 hours. The PES particles were then put into the PVDF solution prepare for PVDF/PES solution by stirring the mixture (magnetic stirrer, HJ-6A, Gongyi Yuhua Instrument Co. Ltd.) under ambient temperature for 2 hours. Concentrations of PVDF/PES solution were listed in tab. 1.

This paper applies electrospinning to study the mechanism of dropping. The PVDF/PES solution was put into a 10 mL syringe, other parameters were listed in tab. 2.

Table 1. The PVDF/PES solutions with different concentrations

PVDF [g]	PES [g]	DMF [g]	Acetone [g]	Concentration [%]
0.2	0.2	13.72	5.88	2
0.3	0.3	13.58	5.82	3
1	1	12.6	5.4	10
1.5	1.5	11.9	5.1	15

Table 2. Spinning parameters and average diameter, receptor distance, *L*, rate of solution supply, *Q*, PVDF/PES concentration, *c*, and average diameter, *d*

Samples	Voltage [kV]	L [cm]	Q [mLh^{-1}]	c [%]	d [nm]
1	15	1	0.5	3%	–
2	17	3	0.5	3%	–
3	19	5	0.5	3%	–
4	15	15	0.5	3%	739±55.44
5	15	17	0.5	3%	870±76.33
6	15	19	0.5	3%	1045±93.89
7	17	17	0.5	3%	507±26.56
8	19	17	0.5	3%	492±31.07
9	17	15	0.1	3%	525±34.81
10	17	15	0.3	3%	570±29.38
11	17	15	0.5	3%	856±43.38
12	17	17	0.5	10%	91±4.88
13	17	17	0.5	15%	508±24.15

Results and discussions

During the spinning process, we put a piece of sheet glass between the needle and the receptor to identify the possible dropping process. When the glass was put 1 cm and 3 cm, respectively, before the needle for Samples 1 and 2, only aggregated fibers were observed, figs. 2(a) and 2(b), respectively, when it was put 5 cm before the needle, we could observe micro spheres, see fig. 2(c) dropping point was near 5 cm from the needle.

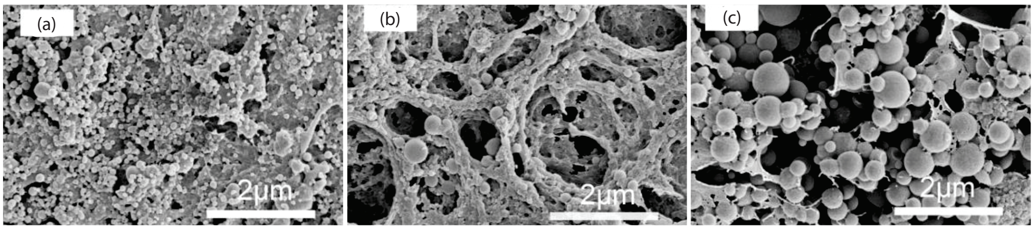

Figure 2. The SEM illustrations using a glass receptor to identify the dropping point; (a) 1 cm, (b) 3 cm, and (c) 5 cm from the needle for Samples 1-3, respectively

When the receptor is put after the dropping point, particles can be obtained, and the receptor distance will great affect the particle size. A longer distance implies a less electric field strength, as a result, a smaller acceleration is obtained for the ejecting jet, which has a lower velocity, and according to the mass conservation given in eq. (1), the radius of the moving jet at the dropping point is larger, as a result, a larger particles can be predicted as illustrated in fig. 3. The average diameters for Samples 4-6 are, respectively, 739 nm, 870 nm, and 1045 nm, while their receptor distances are, respectively, 15 cm, 17 cm, and 19 cm.

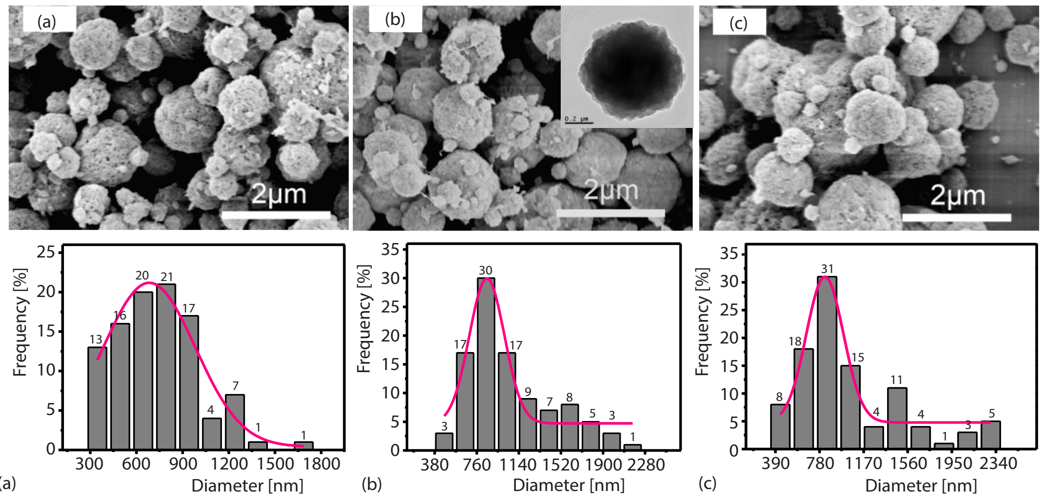

Figure 3. The SEM and TEM image of effect of receptor distance on particle size (a)-(c) for Samples 4-6, respectively

The strength of the electric field, E, is inversely proportional to the receptor distance, L:

$$E \propto \frac{1}{L} \tag{3}$$

The ejecting acceleration, a, is proportional to E:

$$a \propto E \tag{4}$$

A higher acceleration means a higher ejecting velocity:

$$u \propto a \tag{5}$$

According to eq. (1), the square of the diameter of jet at the dropping point is inversely proportional to the velocity:

$$d^2 \propto \frac{1}{u} \tag{6}$$

The sphere diameter, D, scales with d:

$$D \propto d \tag{7}$$

By previous simple qualitative analysis, we have:

$$D^2 \propto L \tag{8}$$

or

$$D = \sqrt{\alpha_1 + \beta_1 L} \tag{9}$$

where α_1 and β_1 are constants which can be determined experimentally:

$$D = \sqrt{136000L - 1521740} \tag{10}$$

where D is in nanometer and L cm, fig. 8.

The rate of solution supply also affects greatly the dropping process, according to eq. (1):

$$d^2 \propto Q \tag{11}$$

By aforementioned similar analysis, the effect of flow rate on microsphere diameter can be expressed:

$$D = \sqrt{\alpha_2 + \beta_2 Q} \tag{12}$$

where α_2 and β_2 are constants which can be determined experimentally:

$$D = \sqrt{100000 + 1142777Q} \tag{13}$$

where Q is in mL/h.

Figure 8 reveals that a higher flow rate, Q, implies a larger diameter of microspheres. During the dropping process, daughter jets might be ejected from the dropping point. A daughter jet might link to a drop, as a result, nanofiber-sphere structure can be observed as the cases given in figs. 4(a) and 4(b), and figs. 5(b) and 5(c).

The voltage affects particle size greatly, a higher voltage means a higher velocity of the moving jet, and smaller particles can be obtained as illustrated in fig. 9.

We assume that the jet velocity scales with the applied voltage:

$$V \propto u \tag{14}$$

Similar to the previous analysis, the square of diameter of the microspheres is inversely proportional to u:

$$D^2 \propto \frac{1}{u} \propto \frac{1}{V} \tag{15}$$

or

$$D = \sqrt{\alpha_3 + \frac{\beta_3}{V}} \tag{16}$$

where α_3 and β_3 are constants which can be determined experimentally.

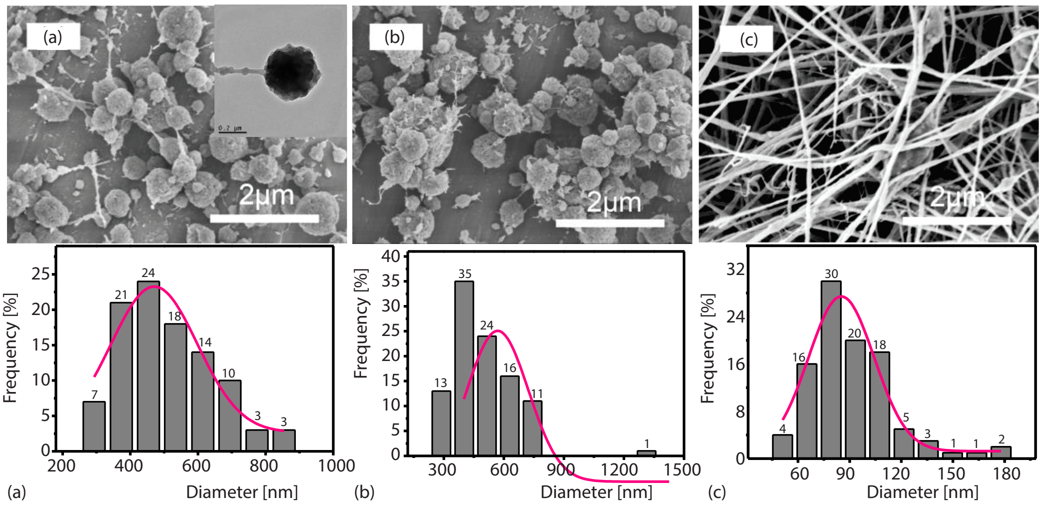

Figure 4. The SEM and TEM image of nanofiber-sphere structure in dropping process (a)-(c) for Samples 7, 8, and 12, respectively

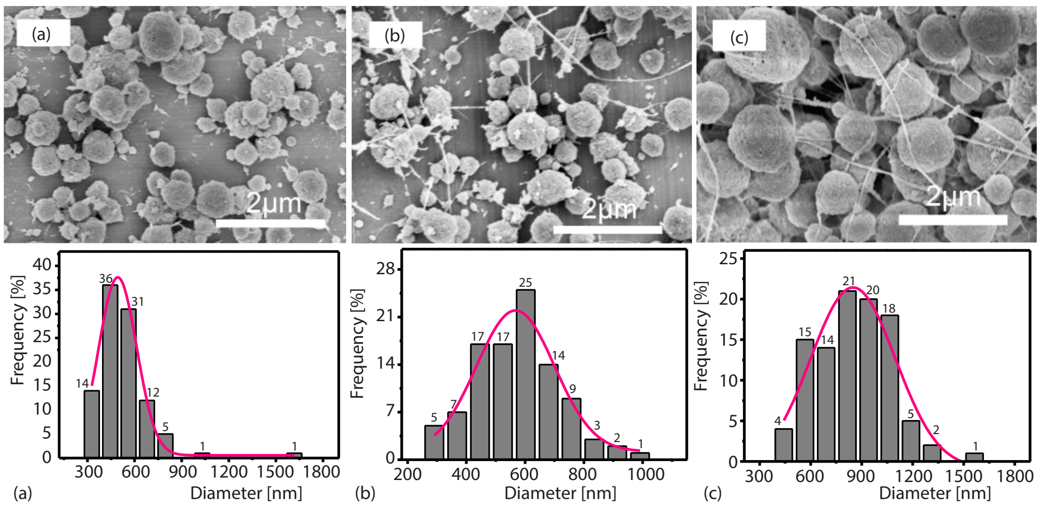

Figure 5. The SEM image of dropping *vs.* spinning (a)-(c) for Samples 9-11, respectively

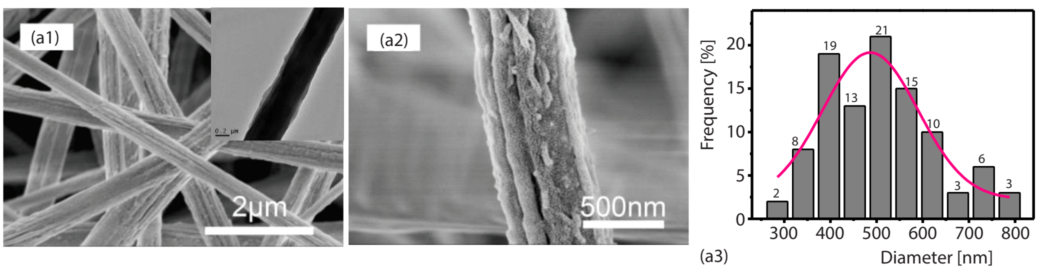

Figure 6. The SEM and TEM image of unsmooth surface due to fast solvent evaporation for Sample 13

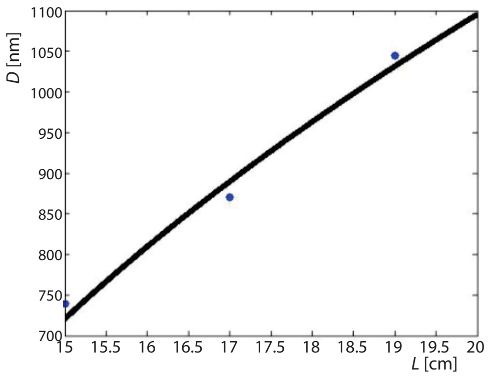

Figure 7. Theoretical prediction of fiber diameter (dots are experiment results)

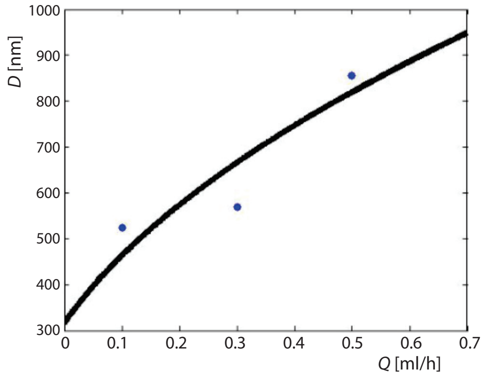

Figure 8. Effect of flow rate on microsphere size (dotes are experimental data, continuous line is the theoretical prediction)

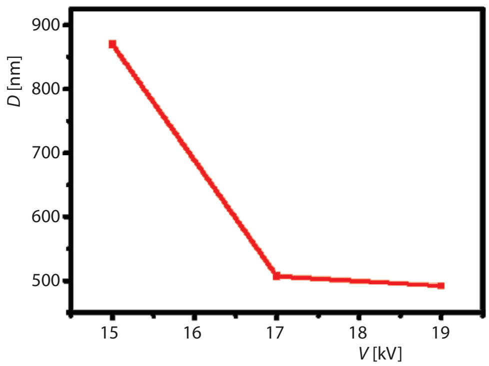

Figure 9. Effect of applied voltage on microsphere size

With increase of PVDF/PES concentration, viscous coefficient increases, according to eq. (2), dropping process is difficult to take place, as a result, fibers can be obtained as illustrated in fig. 4(c). If concentration further increases, solvent decreases, no dropping will happen, and a fast solvent evaporation will result in unsmooth surface of the fiber as illustrated in figs. 4(c) and 6.

Generally a higher polymer concentration results in a higher viscous coefficient:

$$\mu \propto c^b \tag{17}$$

where b is a scaling parameter. According to eq. (2), a higher viscous coefficient leads to a longer delayed dropping process. When the receptor is fixed, dropping process will disappear for higher polymer concentrations as for the Samples 12 and 13, see fig. 4(c), fig. 6.

In previous analysis we use Newtonian flow, non-Newtonian flow can also explain the experimental phenomena. We write down a non-Newtonian model to replace eq. (2):

$$T = \pi r^2 \left\{ \mu \frac{\mathrm{d}u}{dx} + \lambda \left(\frac{\mathrm{d}u}{\mathrm{d}x} \right)^3 \right\} \tag{18}$$

where λ is a non-Newtonian coefficient, we obtain similar theoretical formulae with different values of α_i and β_i (i = 1~3). We can also update the scaling laws given in eqs. (3) and (14) in a more complex forms:

$$E \propto \frac{1}{L^m} \tag{19}$$

$$V \propto u^n \tag{20}$$

where m and n are positive numbers larger than 1. Similar theoretical formulae with different values of α_i and β_i (i = 1~3) can be obtained.

Conclusions

In this paper we give a theoretical analysis of the dropping process in the electrospinning, when the moving jet meets the following condition:

$$T = \pi r^2 \mu \frac{\mathrm{d}u}{\mathrm{d}x} = \mu \frac{Q}{\rho u}\frac{\mathrm{d}u}{\mathrm{d}x} = \mu \frac{Q}{\rho}\frac{\mathrm{d}}{\mathrm{d}x}(\ln u) << 1 \tag{21}$$

dropping occurs.

Low polymer concentration (small μ), low flow rate (small Q), high density (large ρ) are main factors for producing microspheres, and the receptor's distance and the applied voltage can be effectively used to control the microsphere size. The solvent system is the main factor to produce porous microsphere, sudden solvent evaporation can result in porous microsphere. According to the mass equation, solvent evaporation [15, 16] will also affect the microsphere size, we will discuss this in a forthcoming paper. By controlling the dropping parameters, we can also produce microsphere-fiber blends with tenable porosity for biomimic design of nanofiber membrane with maximal air permeability [17, 18] like that of silkworm cocoons [19], and can revivify the lost technology of Fangzhu, which is to catch water from air [20]. The present theory is also valid for other spinning methods like the bubble electrospinning [1, 3, 10, 11, 14, 16].

Acknowledgement

The work is supported by Science and Technology Project of Suzhou City in China under grant No. SYG201827, National Natural Science Foundation of China under grant No. 51802244, Priority Academic Program Development of Jiangsu Higher Education Institutions (PAPD).

References

[1] He, J.-H., *et al.*, Review on Fiber Morphology Obtained by the Bubble Electrospinning and Blown Bubble Spinning, *Thermal Science*, *16* (2012), 5, pp. 1263-1279
[2] Reyderman, L., Stavchansky, S., Electrostatic Spraying and Its Use in Drug-Delivery Cholesterol Microspheres, *International Journal of Pharmaceutics*, *124* (1995), 1, pp. 75-85
[3] Yin, J., *et al.,* Numerical Approach to High-Throughput of Nanofibers by a Modified Bubble-Electrospinning, *Thermal Science*, *24* (2020), 4, pp. 2367-2375
[4] Ahmed, A., Xu, L., Numerical Analysis of the Electrospinning Process for Fabrication of Composite Fibers, *Thermal Science*, *24* (2020), 4, pp. 2377-2383
[5] Li, F., *et al.,* A Hierarchical Hybrid Electrode for Rapid Oxygen Reduction Reaction below 800 °C, *Thermal Science*, *24* (2020), 4, pp. 2455-2462
[6] Li, X. X., *et al.,* Nanofibers Membrane for Detecting Heavy Metal Ions, *Thermal Science*, *24* (2020), 4, pp. 2463-2468
[7] Li X. X., *et al.*, The Effect of Sonic Vibration on Electrospun Fiber Mats, *Journal of Low Frequency Noise Vibration and Active Control, 38* (2019), 3-4, pp. 1246-1251
[8] Zhao, J. H., *et al.,* Needle's Vibration in Needle-Disk Electrospinning Process: Theoretical Model and Experimental Verification, *Journal of Low Frequency Noise Vibration and Active Control, 38* (2019), 3-4, pp. 1338-1344
[9] Wu, Y. K., Liu, Y., Fractal-Like Multiple Jets in Electrospinning Process, *Thermal Science*, *24* (2020), 4, pp. 2499-2505
[10] He, J. H., Advances in Bubble Electrospinning, *Recent Patents on Nanotechnology*, *13* (2019), 3, pp. 162 -163
[11] He, J. H., Liu, Y. P., Bubble Electrospinning: Patents, Promises and Challenges, *Recent Patents on Nanotechnology*, *14* (2020), 1, pp. 3-4
[12] He, C. H., *et al.,* Taylor Series Solution for Fractal Bratu-Type Equation Arising in Electrospinning Process, *Fractals*, *28* (2020), 1, 2050011

[13] He, J. H., On the Height of Taylor Cone in Electrospinning, *Results in Physics*, *17* (2020), June, 103096
[14] Sun, Q. L., *et al.,* Jet Speed in Bubble Rupture, *Thermal Scienc*e, *22* (2018), 1A, pp. 47-50
[15] Peng, N. B., *et al.*, A Rachford-Rice Like Equation for Solvent Evaporation in the Bubble Electrospinning, *Thermal Science*, *22* (2018), 4, pp. 1679-1683
[16] Li, X. X., *et al.*, Bubble Electrospinning with an Auxiliary Electrode and an Auxiliary Air-Flow, *Recent Patents on Nanotechnology*, *14* (2020), 1, pp. 42-45
[17] Liu, Y. Q., *et al.,* Air Permeability of Nanofiber Membrane with Hierarchical Structure, *Thermal Science*, *22* (2018), 4, pp. 637-1643
[18] Peng, N. B., He, J. H., Insight into the Wetting Property of a Nanofiber Membrane by the Geometrical Potential, *Recent Patents on Nanotechnolog*y, *14* (2020), 1, pp. 64-70
[19] Liu, F. J., *et al.,* Silkworm (Bombyx Mori) Cocoon *vs*. Wild Cocoon: Multi-Layer Structure and Performance Characterization, *Thermal Science*, *23* (2019), 4, pp. 2135-2142
[20] He, C. H., *et al.,* Fangzhu: An Ancient Chinese Nanotechnology for Water Collection from Air: History, Mathematical Insight, Promises and Challenges, *Mathematical Methods in the Applied Sciences*, On-line first, https://doi.org/10.1002/mma.6384, 2020

Paper submitted: December 28, 2019
Paper revised: June 2, 2020
Paper accepted: June 2, 2020